Synthesis of Atomically Thin 1T-TaSe₂ with a Strongly Enhanced Charge-Density-Wave Order

Hong Wang, Yu Chen, Chao Zhu, Xuewen Wang, Hongbo Zhang, Siu Hon Tsang, Hongling Li, Jinjun Lin, Ting Yu,* Zheng Liu,* and Edwin Hang Tong Teo*

Bulk 1T-TaSe₂ as a charge-density-wave (CDW) conductor is of special interest for CDW-based nanodevice applications because of its high CDW transition temperature. Reduced dimensionality of the strongly correlated material is expected to result in significantly different collective properties. However, the growth of atomically thin 1T-TaSe₂ crystals remains elusive, thus hampering studies of dimensionality effects on the CDW of the material. Herein, chemical vapor deposition (CVD) of atomically thin TaSe₂ crystals is reported with controlled 1T phase. Scanning transmission electron microscopy suggests the high crystallinity and the formation of CDW superlattice in the ultrathin 1T-TaSe₂ crystals. The commensurate–incommensurate CDW transition temperature of the grown 1T-TaSe₂ increases with decreasing film thickness and reaches a value of 570 K in a 3 nm thick layer, which is 97 K higher than that of previously reported bulk 1T-TaSe₂. This work enables the exploration of collective phenomena of 1T-TaSe₂ in the 2D limit, as well as offers the possibility of utilizing the high-temperature CDW films in ultrathin phase-change devices.

Dr. H. Wang, Dr. H. Li, J. Lin, Prof. E. H. T. Teo
School of Electrical and Electronic Engineering
Nanyang Technological University
Singapore 639798, Singapore
E-mail: htteo@ntu.edu.sg

Dr. Y. Chen, H. Zhang, Prof. T. Yu
Division of Physics and Applied Physics
School of Physical and Mathematical Sciences
Nanyang Technological University
Singapore 637371, Singapore
E-mail: yuting@ntu.edu.sg

Dr. C. Zhu, Prof. Z. Liu, Prof. E. H. T. Teo
School of Materials Science and Engineering
Nanyang Technological University
50 Nanyang Avenue, Singapore 639798, Singapore
E-mail: z.liu@ntu.edu.sg

Prof. X. Wang
Institute of Flexible Electronics
Northwestern Polytechnical University
Xi'an 710072, China

Dr. S. H. Tsang
Temasek Laboratories@NTU
Nanyang Technological University
Singapore 637553, Singapore

1. Introduction

Charge density wave (CDW) is an ordered state characterized by an electron density modulation and an accompanying periodic lattice distortion.[1] CDW as a collective phenomenon is fundamentally important for studying many-body physics and some correlated phenomena such as superconductivity.[2,3] Moreover, the switching between CDW and other states could be utilized for applications such as ultrafast memories, oscillators, and logic circuits.[4–7] A critical requirement for CDW application is that the material should exhibit high transition temperature to CDW symmetry-reducing phases. Some 2D transition metal dichalcogenides (TMDCs) such as 1T-TaSe₂ and 1T-TaS₂, which have high transition temperatures near or above room temperature, are good candidates and hold great potential for device applications.[4–6,8] Particularly, 1T-TaSe₂ in its original structure has a trigonal D^3_{3d} space-group symmetry, where each Ta atom is octahedrally coordinated by six Se atoms. Bulk 1T-TaSe₂ is in an incommensurate CDW (ICCDW) state when the temperature is between 473 and 600 K, and transforms to a commensurate CDW (CCDW) state with a superlattice of $(13)^{1/2} a_0 \times (13)^{1/2} a_0$ rotated 13.9° from the unreconstructed unit cell when the temperature is below 473 K.[9] On the other hand, TaSe₂ can exist in other structures including the 2H and 3R phases. For instance, 2H-TaSe₂ as a more stable phase has a D^4_{6h} space-group symmetry, where each Ta atom is coordinated by six Se atoms in a trigonal prismatic arrangement. Compared with the 1T phase, the undistorted lattice of 2H-TaSe₂ undergoes an incommensurate CDW transition at $T_{ICCDW} = 122$ K, followed by a commensurate CDW transition at $T_{CCDW} = 90$ K, which is much lower than the T_{CCDW} of 1T-TaSe₂.[9] Moreover, when the thickness of the bulk 1T-TaSe₂ is further reduced to the 2D limit, the CDW of the resulting ultrathin product is expected to exhibit promising properties toward thin-film-based CDW applications.[6,10,11] Therefore, developing an effective strategy for controlled synthesis of ultrathin 1T-TaSe₂ while preventing the formation of 2H, 3R, and 1H (as the monolayer form of 2H or 3R) phases is of high importance for both fundamental research and practical applications.

Recently, ambient-pressure chemical vapor deposition (CVD) has been demonstrated to be capable of producing a number

of TMDC layers on substrates.[12–21] Robust CDW order and enhanced superconducting order were observed in CVD grown ultrathin 2H- and 3R-TaSe$_2$, respectively.[22,23] However, the synthesis of mono- and few-layer TaSe$_2$ with the metastable 1T phase is still a challenging task and currently can only be achieved by molecular beam epitaxy (MBE) under ultrahigh vacuum (UHV, base pressure = 2×10^{-10} Torr).[11] Such severe growth requirements limit the exploration of novel 2D CDW phase transitions in 1T-TaSe$_2$ and related nanodevices.

Here we demonstrate the ambient-pressure CVD growth of TaSe$_2$ atomic layers with controlled 1T or 1H phase by using Mg salts as growth promoters. The 1T phase percentage in the product has a strong correlation with the deposition temperature. Scanning transmission electron microscopy (STEM) suggests the formation of CDW superlattice in the high-crystalline 1T-TaSe$_2$ layers. Temperature-dependent Raman spectroscopy is used to study the phase transition from CCDW to ICCDW in 1T-TaSe$_2$. A transition temperature of 570 K is observed in a 3 nm thick 1T-TaSe$_2$, which is 97 K higher than that of previously reported bulk samples. Moreover, additional CDW-related soft modes observed in the Raman spectra of monolayer 1T-TaSe$_2$ provide strong evidence that CCDW survives in the 2D limit of 1T-TaSe$_2$.

2. Results and Discussion

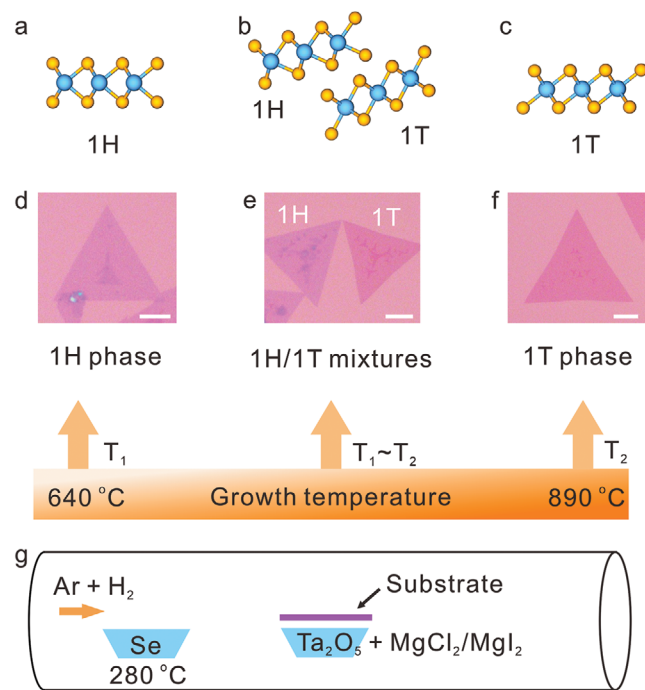The side view of the atomic structures of the 1H phase, 1H/1T mixtures, and 1T phase of TaSe$_2$ is shown in **Figure 1**a–c. A

Figure 1. Illustration of the phase-controlled synthesis of atomically thin 1H- and 1T-TaSe$_2$ crystals. The upper panels show the a–c) atomic structures and d–f) typical optical images of 1H phase, 1H plus 1T, and 1T phases of TaSe$_2$. The monolayer 1T-TaSe$_2$ appears red while 1H-TaSe$_2$ shows slightly blue. The small few-layer nuclei on each triangle are redder (bluer) than the underlying monolayer 1T (1H) crystal. g) The schematic representation of the CVD growth chamber. High substrate temperature favors the growth of 1T-TaSe$_2$. The scale bars in panels (d)–(f) are 10 μm.

schematic of the CVD reactor is shown in the bottom panel of Figure 1 (see also Experimental Section for details). Typically, Ta$_2$O$_5$ and MgCl$_2$ or MgI$_2$ are mixed in an alumina boat and used as the Ta precursors for the growth of atomically thin TaSe$_2$ on the nearby SiO$_2$/Si substrates. We note that Ta$_2$O$_5$ alone, which has a melting point of 1872 °C, cannot be vaporized and will not result in any nucleation of TaSe$_2$ in our experiment. The mechanism of molten-salt-assisted CVD growth of TMDC layers has been investigated in previous studies.[24–26] Briefly, at a temperature higher than the melting point of salts, the Ta$_2$O$_5$ powders dissolve in the molten salts (such as MgCl$_2$) and react with the latter to form tantalum oxychlorides, which are gaseous at the CVD growth temperature and further react with selenium vapor to form TaSe$_2$ on substrates. It should be noted that 1T-TaSe$_2$ as a high-temperature phase is metastable at room temperature.[9,27] Therefore, rapid cooling upon completion of the growth should be applied for preparing 1T-TaSe$_2$.[9,28] We also observed that the growth temperature had a significant influence on the polytypes of TaSe$_2$. A relatively high temperature of 890 °C tends to produce 1T-TaSe$_2$ while a much lower temperature of 640 °C results in the 1H-TaSe$_2$. In between these two temperatures, 1H- and 1T-TaSe$_2$ mixtures are obtained (Figure 1d–f). First principles calculation on monolayer TaSe$_2$ suggests that the total energy per unit cell of the 1T phase is higher than that of the 1H phase.[29] Therefore, higher substrate temperature facilitates the growth of 1T phase TaSe$_2$ while lower temperature favors the formation of 1H phase.

The variation of the percentage of 1T and 1H phase in the product against the growth temperature was systematically studied from 640 to 890 °C. Raman spectroscopy was used to identify the two different phases since each phase has unique Raman peaks at room temperature. **Figure 2**a shows the typical Raman spectra of monolayer 1H- and 1T-TaSe$_2$ grown by CVD. For 1H-TaSe$_2$ which has no lattice distortion at room temperature, the prominent Raman peaks observed at 232 and 216 cm^{-1} match well with the out-of-plane vibrational A$_{1g}$ mode and in-plane vibrational E$_{2g}$ mode of bulk 2H-TaSe$_2$, respectively. The broad peak centered at about 140 cm^{-1} could be assigned to a two-phonon process in 2H-TaSe$_2$.[9,30–32] In comparison, the monolayer 1T-TaSe$_2$ shows A$_{1g}$-symmetry peak at 185 cm^{-1} and strong CCDW superlattice-related peaks near or below 105 cm^{-1} at room temperature.[9,30] Furthermore, the absence of 1H (1T) peaks in the Raman spectrum of 1T (1H) TaSe$_2$ sample indicates that the ultrathin TaSe$_2$ crystals grown are of high purity, which are difficult to achieve according to previous reports.[27]

As an identification tool, Raman spectroscopy verifies that monolayer 1T-TaSe$_2$ is much redder than monolayer 1H-TaSe$_2$ (which appears slightly blue) under optical microscope examination. Typical optical images of TaSe$_2$ crystals grown at different temperatures are shown in Figure 2b–d. Atomic force microscopy (AFM) measurement (inset of Figure 2b) suggests the typical thickness of the TaSe$_2$ crystal is around 1.3 nm. Considering that the surface of ultrathin metallic TaSe$_2$ is easy to be oxidized during AFM measurement in air, the thickness of 1.3 nm could be assigned to a monolayer.[33] By analyzing the deposited thin crystals with Raman spectroscopy, the 1T and 1H phase percentages at different growth temperatures are estimated (Figure 2e). At 890 °C, the 1T phase is the majority phase and the percentage is about 95%. In the range of 890–640 °C,
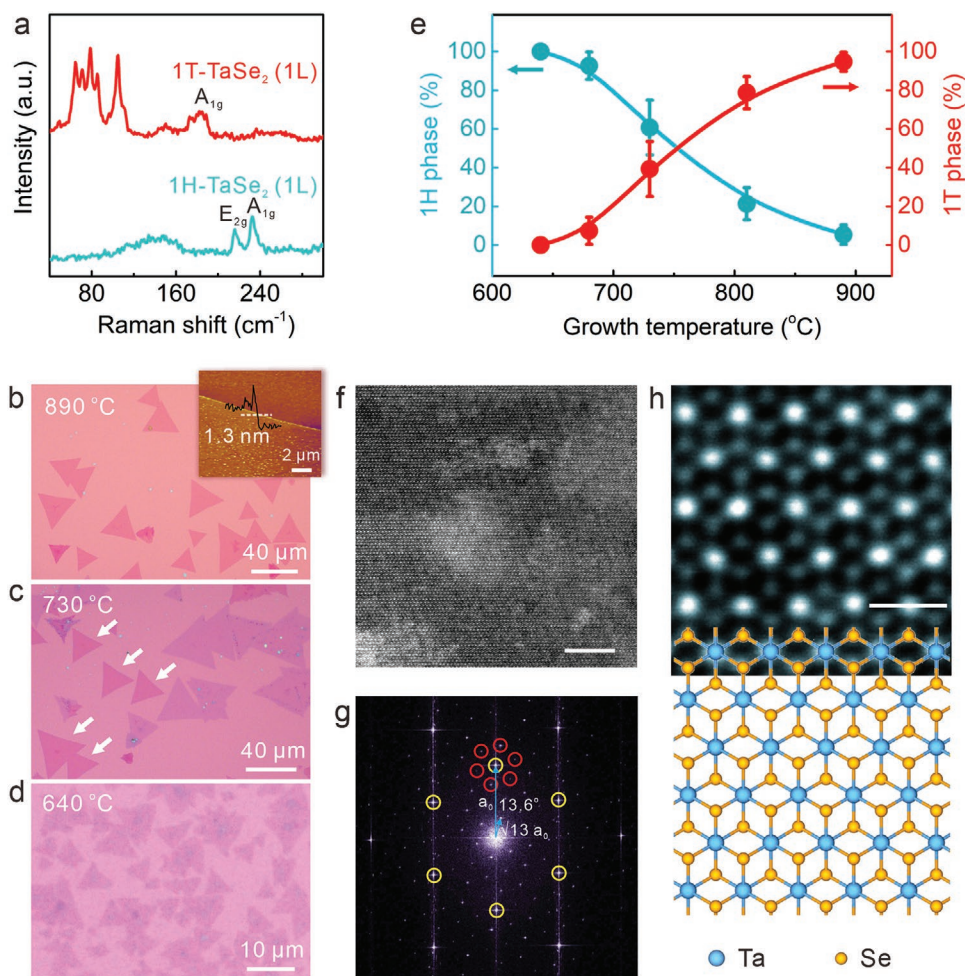
Figure 2. Phase evolution of ultrathin TaSe$_2$ crystals and STEM characterization of 1T-TaSe$_2$. a) Room-temperature Raman spectra of monolayer 1H- and 1T-TaSe$_2$. b–d) Representative optical images of the products grown at b) 890 °C, c) 730 °C, and d) 640 °C. A representative AFM image (inset of panel (b)) shows the typical thickness is 1.3 nm. The 1T phase crystals are indicated with white arrows in panel (c). e) Substrate temperature-dependent phase evolution in the CVD growth. f) HAADF–STEM image and g) corresponding FFT pattern of the 1T-TaSe$_2$ layers. 1T-TaSe$_2$ shows stripe or superlattice in the real space and satellite peaks in the reciprocal space due to CCDW formation. Scale bar is 5 nm in panel (f). h) Atomic resolution HAADF–STEM image of 1T-TaSe$_2$ layers overlaid with the atomic model. Scale bar is 0.5 nm in panel (h).

the 1T phase percentage decreases with decreasing temperature while the 1H phase percentage increases. Additionally, Raman maps shown in Figure S1 (Supporting Information) confirm the uniformity of the sample in each crystal. It is noted that by using molten salt-assisted CVD growth of TMDC, the growth temperature should be around or higher than the melting point of salt. Indeed, we observed no nucleation of TaSe$_2$ on substrates below 700 °C with MgCl$_2$. However, at the lowest effective growth temperature with MgCl$_2$, there is still a large percentage of 1T phase in the product. To prepare the sole 1H phase, the growth temperature should be further reduced. Therefore, MgI$_2$, which has a lower melting point of 637 °C, is used as the promoter, and when the growth temperature decreases to 640 °C, sole 1H phase TaSe$_2$ crystals are obtained on substrates (Figure 2d). Raman spectra of monolayer 1T and 1H TaSe$_2$ grown at different temperatures are shown in Figure S2 (Supporting Information). We also studied the effect of other salts including NaCl, CaCl$_2$, and KI (Figure S3, Supporting Information) and identified Mg salts as the most active

promoters for growing atomically thin TaSe$_2$ crystals with uniform thickness.

STEM was performed to analyze the crystallographic structure and to observe the CCDW-related superlattice in as-grown 1T-TaSe$_2$. After examined by Raman spectroscopy, the 1T-TaSe$_2$ layers grown on SiO$_2$/Si substrates were transferred to a Cu grid by a polymethyl methacrylate (PMMA)-assisted transfer method.[34] Figure 2f shows the large field of view of high-angle annular-dark-field (HAADF)–STEM image of 1T-TaSe$_2$ layers acquired at room temperature. An obvious feature that could be observed in the image is the periodic stripes or superlattice fringes, which result from the CCDW-related lattice distortion. Correspondingly, the fast Fourier transform (FFT) pattern of Figure 2f confirms the satellite spots (marked by red circles in Figure 2g) of the CCDW-related superlattice that surround the main sixfold symmetry spots (marked by yellow circles) of the fundamental 1T lattice.[35–37] In addition, these two sets of spots have the relative rotation angle of 13.6° and length ratio of $(13)^{1/2}$:1 (Figure 2g), in good accordance with other

**ADVANCED
SCIENCE NEWS**

www.advancedsciencenews.com

**ADVANCED
FUNCTIONAL
MATERIALS**

www.afm-journal.de

literatures.[9,11] As a comparison, the FFT pattern (Figure S4, Supporting Information) of hexagonal-phase $TaSe_2$ shows solely the fundamental lattice-related sixfold symmetry features, suggesting the absence of CDW at room temperature. The atomic resolution HAADF-STEM image of $1T$-$TaSe_2$ shown in Figure 2h could be fitted perfectly by the $1T$ structural model, where the octahedral coordination of every Ta atom with the nearest six Se atoms is formed, suggesting that the sample crystallizes in $1T$ structure with good quality.

The chemical states of the as-grown ultrathin $1T$-$TaSe_2$ crystals were examined by X-ray photoemission spectroscopy (XPS) (Figure S5, Supporting Information). The high-resolution Se 3d core-level spectrum could be fitted with Se $3d_{5/2}$ (53.3 eV) and Se $3d_{3/2}$ (54.1 eV) peaks in agreement with the spectra of $TaSe_2$ (Figure S5a, Supporting Information).[22] The high-resolution Ta 4f core-level spectrum (Figure S5b, Supporting Information) could be fitted with components corresponding to $TaSe_2$ (binding energy 22.6 eV, full width at half maximum (FWHM) 1.4 eV, Ta $4f_{7/2}$; 24.4 eV, FWHM 1.4 eV, Ta $4f_{5/2}$) and oxidized Ta (25.6 eV, FWHM 2.5 eV, Ta $4f_{7/2}$; 27.6 eV, FWHM 2.5 eV, Ta $4f_{5/2}$). It is noted that thin metallic TMDC layers are easy to be oxidized in air.[38,39] Therefore, the detection of partially oxidized Ta on the surface of ultrathin $TaSe_2$ by XPS is quite reasonable.

Variable-temperature Raman spectroscopy is used to investigate the CDW phase transition in ultrathin $1T$-$TaSe_2$. To avoid oxidation, $1T$-$TaSe_2$ samples were sealed in a small chamber in a glove box under Ar immediately after CVD growth and then shifted to a Raman chamber operated under vacuum. The Raman spectra were first recorded at different temperatures increasing from 80 to 585 K, and then the spectra were taken with decreasing temperature. The temperature dependence of the Raman spectra for a heating cycle of a 10.4 nm thick $1T$-$TaSe_2$ is displayed in **Figure 3**a. At 80 K, at least three distinctive modes are seen clearly at 64, 72, and 97 cm^{-1}. The temperature dependence of the phonon frequencies is presented in Figure 3b. Two strong modes (72 and 97 cm^{-1} at 80 K) of A_g symmetry both soften (frequency downshift) and weaken substantially as the temperature approaches 490 K from below. These two modes behave like the "soft modes" or "critical modes," which associate with the structural distortions during the commensurate to incommensurate transition.[9,30,40,41] By examining the evolution of the well-resolved "soft mode" at 97 cm^{-1} (at 80 K),[9] we conclude that the CDW in a 10.4 nm thick $1T$-$TaSe_2$ is incommensurate above 490 K and commensurate below 490 K. Additionally, as the temperature drops to 490 K and below during the cooling process, the broad peak (centered at 61 cm^{-1}) at 510 K splits into several separated peaks, whose intensities increase with decreasing temperature and reach almost the same values with those of the heating cycle at room temperature (Figure 3c). The recovery of the commensurate state suggests that the sample was not oxidized during the heating cycle.

The temperature-dependent Raman spectra and phonon frequencies of 6.3 and 3 nm thick $1T$-$TaSe_2$ are shown in **Figure 4**. In the 3 nm thick $TaSe_2$, both of the "soft modes," exclusive to the commensurate CDW state, are also observed and follow the same evolution as observed in the 10.4 nm thick sample. It is remarkable that for the thinner samples, the well-resolved higher energy "soft mode" survives up to
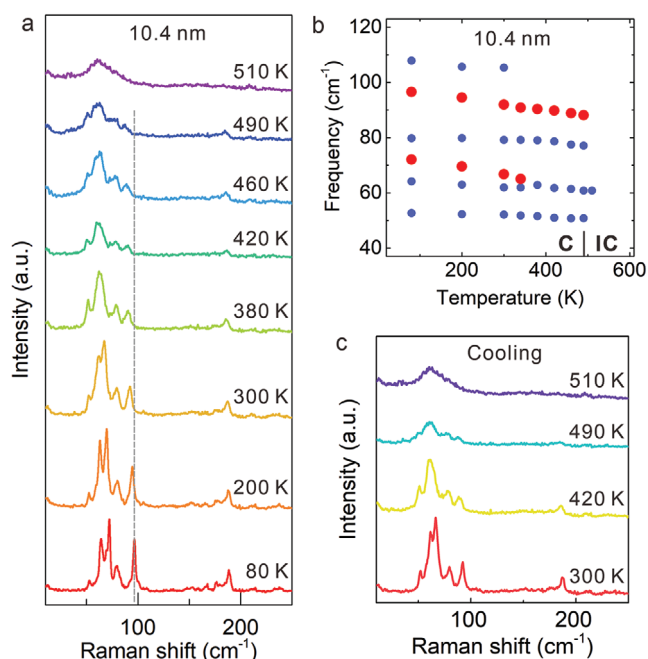

Figure 3. Raman spectroscopic investigation of the CDW transition in a 10.4 nm thick $1T$-$TaSe_2$. a) Representative Raman spectra of a 10.4 nm thick $1T$-$TaSe_2$ sample at selected temperatures for the heating cycle. b) Temperature dependence of the phonon frequencies of the 10.4 nm thick $1T$-$TaSe_2$. "Soft modes" are indicated with red dots. c) Representative Raman spectra of the same sample at selected temperatures during the cooling cycle.

higher temperatures as compared with the 10.4 nm case. The recovery of the commensurate state in the cooling cycle suggests that the sample has not deteriorated at high temperature up to 585 K (Figure S6, Supporting Information). Based on the temperature dependence of the frequencies of the "soft modes," the commensurate–incommensurate phase transition temperatures are determined to be 520 and 570 K for 6.3 and 3 nm thick $1T$-$TaSe_2$, respectively. The transition temperature of commensurate–incommensurate CDW (T_{CCDW}) is summarized as a function of layer numbers in the phase diagram in **Figure 5**. With decreasing layer thickness of the $TaSe_2$ from 17 to 3 nm, T_{CCDW} increases from 490 to 570 K. Moreover, the T_{CCDW} (570 K) of a 3 nm thick $1T$-$TaSe_2$ is 97 K higher than the previously reported value in bulk $1T$-$TaSe_2$ determined by the same Raman spectroscopic method.[9,30,40] It is noted that the increase of T_{CCDW} becomes noticeable only when the sample thickness is below 10.4 nm. Within such thickness, the dielectric screening is reduced, causing the enhancement of electron–phonon coupling. In a previous study, Xi et al. attributed the strong enhancement of CDW order in atomically thin $2H$-$NbSe_2$ to the strengthened electron–phonon coupling based on a mean field analysis of frequency shift of CDW amplitude mode.[10,42] However, unlike in the case of $2H$-$NbSe_2$, the assignment of CDW amplitude modes in Ta dichalcogenides including $1T$-$TaSe_2$ is still puzzling and controversial.[9,43,44] Also, it remains unclear if the Fermi surface structures are similar in atomically thin and bulk $1T$-$TaSe_2$. Therefore, the mechanism of the strong enhancement of CDW order in atomically thin CVD grown
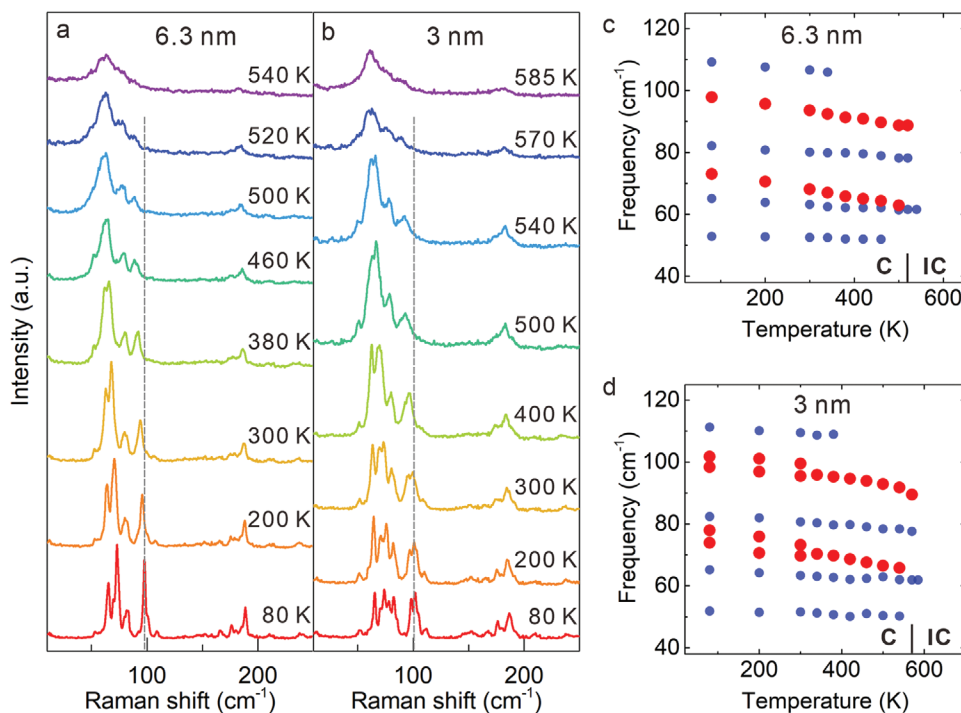
Figure 4. Raman spectroscopic investigation of the CDW transition in 6.3 and 3 nm thick 1T-TaSe$_2$. a,b) Representative Raman spectra of a) 6.3 nm and b) 3 nm 1T-TaSe$_2$ at selected temperatures for the heating cycle. c,d) Temperature dependence of the phonon frequencies of the c) 6.3 nm and d) 3 nm 1T-TaSe$_2$. "Soft modes" are indicated with red dots.

1T-TaSe$_2$ remains to be elucidated by further theoretical and experimental studies.[45]

For the monolayer (1.3 nm thick) 1T-TaSe$_2$, the "soft modes" corresponding to commensurate CDW are observed with frequencies shifted to 80 and 107 cm^{-1} at 80 K, and remain
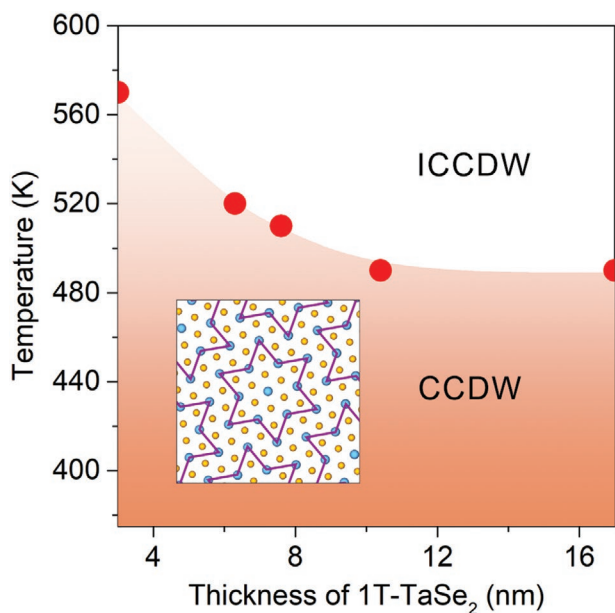

Figure 5. Thickness–temperature phase diagram of 1T-TaSe$_2$ grown by CVD. The inset shows the schematic diagram of the star-of-David CCDW patterns in 1T-TaSe$_2$.

detectable up to a temperature of 500 K (**Figure 6**). However, when the temperature increases to 520 K, the spectrum shows only a very weak and broad feature almost undetectable from the baseline, which is attributed to sample deterioration as the Raman spectra could not recover in the subsequent cooling process (Figure S7, Supporting Information). The sample deterioration could be understood from the fact that compared with few-layers, the monolayer is much more unstable in the high-temperature Raman chamber whose vacuum is achieved only by a rotary vane pump. Therefore, the T_{CCDW} of monolayer could not be determined in our experiment. However, a minimum T_{CCDW} value of 500 K suggests that the CDW order is still enhanced in monolayer 1T-TaSe$_2$ as compared with bulk samples. Besides, since the CDW transition is layer dependent, the small few-layer nuclei on monolayer 1T-TaSe$_2$ (as shown in Figure 1e,f) could have a negative effect on the uniformity of the CDW properties of the material. Therefore, future work is needed to improve the uniformity of the thickness of TaSe$_2$ crystals.

3. Conclusion

In conclusion, phase-controlled growth of atomically thin 1T- and 1H-TaSe$_2$ crystals is realized by Mg-salt-assisted CVD. The TaSe$_2$ polytypes determined by Raman spectroscopy are observed to be closely associated with the substrate temperature. HAADF–STEM confirms the high crystallinity and the existence of CCDW superlattice in 1T-TaSe$_2$. The CCDW–ICCDW transition temperature in a 3 nm thick 1T-TaSe$_2$ is
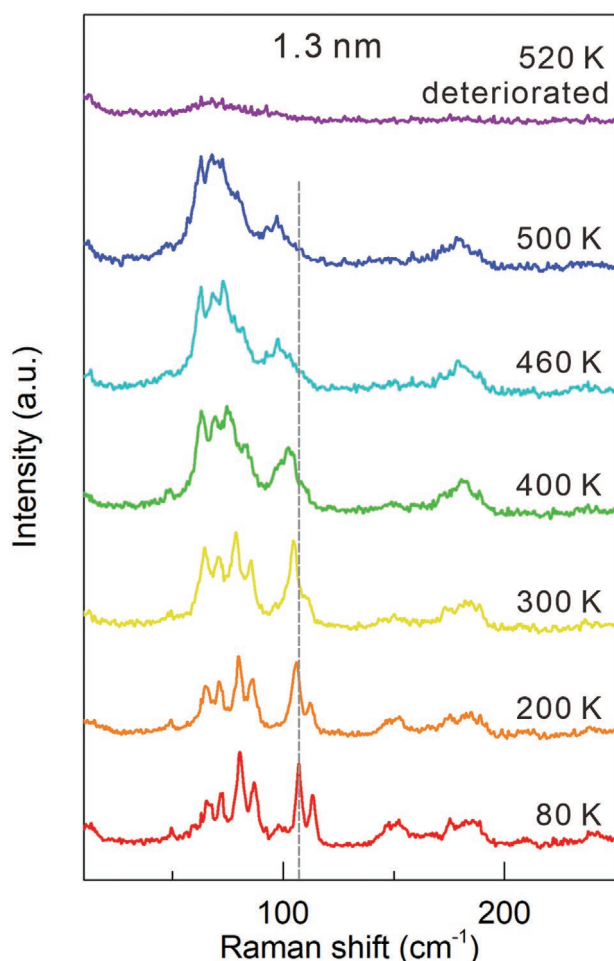
**ADVANCED
SCIENCE NEWS**

www.advancedsciencenews.com

**ADVANCED
FUNCTIONAL
MATERIALS**

www.afm-journal.de

Figure 6. Raman spectroscopic investigation of the CDW transition in a 1.3 nm thick 1T-TaSe$_2$. The sample was deteriorated when the temperature increased to 520 K. "Soft mode" features remain detectable up to 500 K, indicating a minimum T_{CCDW} value of 500 K in the 1.3 nm thick 1T-TaSe$_2$.

nearly 100 K higher than that in previously reported bulk samples, suggesting that the CCDW order is strongly enhanced in atomically thin 1T-TaSe$_2$. This work not only provides an approach for synthesizing ultrathin TaSe$_2$ with controllable phases, but also advances the understanding and engineering of CDW ordering in ultrathin TMDC materials.

4. Experimental Section

Phase-Controlled CVD Growth of TaSe$_2$ Layers: The deposition of atomically thin TaSe$_2$ was conducted in a 1 in. diameter quartz tube heated by a Lindberg/Blue M (TF55035C-1) split-hinge furnace. Ta$_2$O$_5$ (30 mg) and Mg salt (anhydrous MgCl$_2$ or MgI$_2$, 6 mg) powders were thoroughly mixed in an alumina boat and then placed at the center of the furnace. 285 nm SiO$_2$/Si substrate was positioned slightly above the powders with the polished side faced down. For monolayer sample growth, selenium powder located at the upstream of the quartz tube was heated to 280 °C and carried into the furnace center by 40 sccm (cubic centimeters per minute) Ar and 7 sccm H$_2$. After 10 min growth, the growth chamber was rapidly cooled with flowing 140 sccm Ar. After growth, the substrates were cleaned with flowing ethanol to remove possible adsorbed salts.

The percentage of 1T phase in the product was investigated by changing the CVD growth temperature from 640 to 890 °C. For the salt-assisted CVD growth, different Mg salts with different melting points (T_m) were chosen depending on the growth temperature (T_{growth}). For T_{growth} between 700 and 890 °C, MgCl$_2$ ($T_m = 714$ °C) was used as the growth promoter. For T_{growth} between 640 and 690 °C, MgI$_2$ ($T_m = 637$ °C) with the same amount was used. Raman spectroscopy was used to determine the phase percentages of thin crystals grown on substrates. For each growth temperature, three sets of 1T/1H phase percentages were obtained from three repeated experiments, which further gave the standard deviation and the mean value of phase percentage.

1T-TaSe$_2$ samples grown at 890 °C was used for Raman investigations of CDW transitions. Multilayer 1T-TaSe$_2$ samples were prepared by increasing the heating temperature of selenium to about 320 °C, while keeping other growth parameters unchanged.

Characterizations: AFM images and sample thicknesses were measured in tapping mode with an Asylum Research Cypher AFM. HAADF–STEM images were recorded using a probe corrected JEOL ARM200F (S)TEM, operated with the acquisition angle of 68–280 mrad and a convergence angle of about 30 mrad at 80 keV. Transmission electron microscopy (TEM) images of the hexagonal-phase TaSe$_2$ layers were taken by a JEOL JEM-2100 operated at 200 kV. Raman spectra were recorded by a WITec spectrometer (Alpha300, 532 nm laser wavelength) with 50× objective lens and a 2400 lines mm^{-1} grating. The laser power was kept below 0.6 mW. The sample was placed on a Linkam heating/cooling stage in vacuum which allowed the control of the sample temperature during Raman measurements.

Supporting Information

Supporting Information is available from the Wiley Online Library or from the author.

Conflict of Interest

The authors declare no conflict of interest.

[1] R. E. Thorne, *Phys. Today* **1996**, *49*, 42.
[2] M. M. Ugeda, A. J. Bradley, Y. Zhang, S. Onishi, W. Chen, W. Ruan, C. Ojeda-Aristizabal, H. Ryu, M. T. Edmonds, H.-Z. Tsai, A. Riss, S.-K. Mo, D. Lee, A. Zettl, Z. Hussain, Z.-X. Shen, M. F. Crommie, *Nat. Phys.* **2016**, *12*, 92.
[3] Y. I. Joe, X. M. Chen, P. Ghaemi, K. D. Finkelstein, G. A. de la Pena, Y. Gan, J. C. T. Lee, S. Yuan, J. Geck, G. J. MacDougall, T. C. Chiang, S. L. Cooper, E. Fradkin, P. Abbamonte, *Nat. Phys.* **2014**, *10*, 421.

**ADVANCED
SCIENCE NEWS**

www.advancedsciencenews.com

**ADVANCED
FUNCTIONAL
MATERIALS**

www.afm-journal.de

[4] L. Stojchevska, I. Vaskivskyi, T. Mertelj, P. Kusar, D. Svetin, S. Brazovskii, D. Mihailovic, *Science* **2014**, *344*, 177.

[5] I. Vaskivskyi, I. A. Mihailovic, S. Brazovskii, J. Gospodaric, T. Mertelj, D. Svetin, P. Sutar, D. Mihailovic, *Nat. Commun.* **2016**, *7*, 11442.

[6] G. Liu, B. Debnath, T. R. Pope, T. T. Salguero, R. K. Lake, A. A. Balandin, *Nat. Nanotechnol.* **2016**, *11*, 845.

[7] T. Adelman, S. Zaitsev-Zotov, R. Thorne, *Phys. Rev. Lett.* **1995**, *74*, 5264.

[8] X. Wang, H. Liu, J. Wu, J. Lin, W. He, H. Wang, X. Shi, K. Suenaga, L. Xie, *Adv. Mater.* **2018**, *30*, 1800074.

[9] J. Tsang, J. Smith jr., M. Shafer, S. Meyer, *Phys. Rev. B* **1977**, *16*, 4239.

[10] X. Xi, L. Zhao, Z. Wang, H. Berger, L. Forró, J. Shan, K. F. Mak, *Nat. Nanotechnol.* **2015**, *10*, 765.

[11] Y. Chen, W. Ruan, M. Wu, S. Tang, H. Ryu, H.-Z. Tsai, R. Lee, S. Kahn, F. Liou, C. Jia, O. R. Albertini, H. Xiong, T. Jia, Z. Liu, J. A. Sobota, A. Y. Liu, J. E. Moore, Z.-X. Shen, S. G. Louie, S.-K. Mo, M. F. Crommie, *Nat. Phys.* **2020**, *16*, 218.

[12] K. Chen, Z. Chen, X. Wan, Z. Zheng, F. Xie, W. Chen, X. Gui, H. Chen, W. Xie, J. Xu, *Adv. Mater.* **2017**, *29*, 1700704.

[13] L. Zhou, K. Xu, A. Zubair, A. D. Liao, W. Fang, F. Ouyang, Y.-H. Lee, K. Ueno, R. Saito, T. Palacios, J. Kong, M. S. Dresselhaus, *J. Am. Chem. Soc.* **2015**, *137*, 11892.

[14] J. H. Sung, H. Heo, S. Si, Y. H. Kim, H. R. Noh, K. Song, J. Kim, C.-S. Lee, S.-Y. Seo, D.-H. Kim, H. K. Kim, H. W. Yeom, T.-H. Kim, S.-Y. Choi, J. S. Kim, M.-H. Jo, *Nat. Nanotechnol.* **2017**, *12*, 1064.

[15] H. N. Carl, M. P. William, G. Zhaoli, K. Hojin, N. Mehmet, B. W. Robert, Z. T. Liang, K. Youngkuk, E. K. Christopher, S. Frank, Z. Yu Ren, C. Robert, L. Zhengtang, P. Y. Woo, M. R. Andrew, D. Marija, M. K. James, A. T. C. Johnson, *2D Mater.* **2017**, *4*, 021008.

[16] Y. Gao, Z. Liu, D.-M. Sun, L. Huang, L.-P. Ma, L.-C. Yin, T. Ma, Z. Zhang, X.-L. Ma, L.-M. Peng, H.-M. Cheng, W. Ren, *Nat. Commun.* **2015**, *6*, 8569.

[17] Y. Zhou, Y. Nie, Y. Liu, K. Yan, J. Hong, C. Jin, Y. Zhou, J. Yin, Z. Liu, H. Peng, *ACS Nano* **2014**, *8*, 1485.

[18] H. Lin, Q. Zhu, D. Shu, D. Lin, J. Xu, X. Huang, W. Shi, X. Xi, J. Wang, L. Gao, *Nat. Mater.* **2019**, *18*, 602.

[19] L. Liu, J. Wu, L. Wu, M. Ye, X. Liu, Q. Wang, S. Hou, P. Lu, L. Sun, J. Zheng, L. Xing, L. Gu, X. Jiang, L. Xie, L. Jiao, *Nat. Mater.* **2018**, *17*, 1108.

[20] G. H. Han, D. L. Duong, D. H. Keum, S. J. Yun, Y. H. Lee, *Chem. Rev.* **2018**, *118*, 6297.

[21] Y. Zhang, Y. Yao, M. G. Sendeku, L. Yin, X. Zhan, F. Wang, Z. Wang, J. He, *Adv. Mater.* **2019**, *31*, 1901694.

[22] J. Shi, X. Chen, L. Zhao, Y. Gong, M. Hong, Y. Huan, Z. Zhang, P. Yang, Y. Li, Q. Zhang, Q. Zhang, L. Gu, H. Chen, J. Wang, S. Deng, N. Xu, Y. Zhang, *Adv. Mater.* **2018**, *30*, 1804616.

[23] Y. Deng, Y. Lai, X. Zhao, X. Wang, C. Zhu, K. Huang, C. Zhu, J. Zhou, Q. Zeng, R. Duan, Q. Fu, L. Kang, Y. Liu, S. J. Pennycook, X. R. Wang, Z. Liu, *J. Am. Chem. Soc.* **2020**, *142*, 2948.

[24] S. Li, S. Wang, D.-M. Tang, W. Zhao, H. Xu, L. Chu, Y. Bando, D. Golberg, G. Eda, *Appl. Mater. Today* **2015**, *1*, 60.

[25] K. V. Manukyan, K. G. Kirakosyan, Y. G. Grigoryan, O. M. Niazyan, A. V. Yeghishyan, A. G. Kirakosyan, S. L. Kharatyan, *Ind. Eng. Chem. Res.* **2011**, *50*, 10982.

[26] J. Zhou, J. Lin, X. Huang, Y. Zhou, Y. Chen, J. Xia, H. Wang, Y. Xie, H. Yu, J. Lei, D. Wu, F. Liu, Q. Fu, Q. Zeng, C.-H. Hsu, C. Yang, L. Lu, T. Yu, Z. Shen, H. Lin, B. I. Yakobson, Q. Liu, K. Suenaga, G. Liu, Z. Liu, *Nature* **2018**, *556*, 355.

[27] R. Samnakay, D. Wickramaratne, T. R. Pope, R. K. Lake, T. T. Salguero, A. A. Balandin, *Nano Lett.* **2015**, *15*, 2965.

[28] S. Uchida, S. Sugai, *Physica B+C* **1981**, *105*, 393.

[29] J.-A. Yan, M. A. D. Cruz, B. Cook, K. Varga, *Sci. Rep.* **2015**, *5*, 16646.

[30] S. Sugai, K. Murase, S. Uchida, S. Tanaka, *Physica B+C* **1981**, *105*, 405.

[31] S. Sugai, K. Murase, *Phys. Rev. B* **1982**, *25*, 2418.

[32] P. Hajiyev, C. Cong, C. Qiu, T. Yu, *Sci. Rep.* **2013**, *3*, 2593.

[33] H. Wang, Y. Chen, M. Duchamp, Q. Zeng, X. Wang, S. H. Tsang, H. Li, L. Jing, T. Yu, E. H. T. Teo, Z. Liu, *Adv. Mater.* **2018**, *30*, 1704382.

[34] H. Wang, E. J. Sandoz-Rosado, S. H. Tsang, J. Lin, M. Zhu, G. Mallick, Z. Liu, E. H. T. Teo, *Adv. Funct. Mater.* **2019**, *29*, 1902663.

[35] R. Hovden, A. W. Tsen, P. Liu, B. H. Savitzky, I. El Baggari, Y. Liu, W. Lu, Y. Sun, P. Kim, A. N. Pasupathy, L. F. Kourkoutis, *Proc. Natl. Acad. Sci. USA* **2016**, *113*, 11420.

[36] K. Kobayashi, H. Yasuda, *Phys. Rev. B* **2016**, *94*, 201409.

[37] J. Shi, X. Wang, S. Zhang, L. Xiao, Y. Huan, Y. Gong, Z. Zhang, Y. Li, X. Zhou, M. Hong, Q. Fang, Q. Zhang, X. Liu, L. Gu, Z. Liu, Y. Zhang, *Nat. Commun.* **2017**, *8*, 958.

[38] H. Wang, X. Huang, J. Lin, J. Cui, Y. Chen, C. Zhu, F. Liu, Q. Zeng, J. Zhou, P. Yu, X. Wang, H. He, S. H. Tsang, W. Gao, K. Suenaga, F. Ma, C. Yang, L. Lu, T. Yu, E. H. T. Teo, G. Liu, Z. Liu, *Nat. Commun.* **2017**, *8*, 394.

[39] Y. Cao, A. Mishchenko, G. L. Yu, E. Khestanova, A. P. Rooney, E. Prestat, A. V. Kretinin, P. Blake, M. B. Shalom, C. Woods, J. Chapman, G. Balakrishnan, I. V. Grigorieva, K. S. Novoselov, B. A. Piot, M. Potemski, K. Watanabe, T. Taniguchi, S. J. Haigh, A. K. Geim, R. V. Gorbachev, *Nano Lett.* **2015**, *15*, 4914.

[40] J. E. Smith, J. C. Tsang, M. W. Shafer, *Solid State Commun.* **1976**, *19*, 283.

[41] R. Zhao, Y. Wang, D. Deng, X. Luo, W. J. Lu, Y.-P. Sun, Z.-K. Liu, L.-Q. Chen, J. Robinson, *Nano Lett.* **2017**, *17*, 3471.

[42] M. J. Rice, S. Strässler, *Solid State Commun.* **1973**, *13*, 1931.

[43] J. A. Holy, M. V. Klein, W. McMillan, S. Meyer, *Phys. Rev. Lett.* **1976**, *37*, 1145.

[44] J. R. Duffey, R. D. Kirby, R. V. Coleman, *Solid State Commun.* **1976**, *20*, 617.

[45] M. Calandra, *Nat. Nanotechnol.* **2015**, *10*, 737.